DOI https: //doi. org/10.1007/s11595-020-2366-6

Plastic Deformation Mechanism of Dual-phase Steel at Different Strain Rates

PANG Qihang[1,2], ZHAO Zhenduo[3], XU Mei[3*], XU Zhen[1,2*], ZHAO Tan[2]

(1 School of Materials and Metallurgy, University of Science and Technology Liaoning, Anshan 114051, China; 2 State Key Laboratory of Metal Material for Marine Equipment and Application, Anshan Iron & Steel Group Co., Ltd., Anshan 114009, China; 3. State Key Laboratory of Advanced Stainless Steel Materials, Taiyuan Iron & Steel Group Co., Ltd., Taiyuan 030003, China)

Abstract: The mechanical properties of dual-phase steel (DP1000) over the strain rate range of 10^{-3}-10^{3} s^{-1} were studied using an electronic universal testing machine and a high-speed tensile testing machine. The plastic deformation mechanism was investigated from the perspectives of the strain rate sensitivity index, activation volume and dynamic factors. The results show that the tensile strength and yield strength of DP1000 increase as the strain rate increases. The elongation increases without any change after fracture, and then decreased rapidly when the strain rate reaches 10^{3} s^{-1}. The true strain curves of DP1000 show three stages: the point of instability decreases in the strain range of 10^{-3}-10^{-1} s^{-1}; the instability point increases between 10^{0}-5×10^{2} s^{-1}; above 5×10^{2} s^{-1}, and the instability strain becomes smaller again. The plastic deformation mechanism of the DP was determined by the competitive contributions of work hardening (strain hardening, strain rate hardening) and softening effects due to the adiabatic temperature rise.

Key words: dual-phase steel; strain rate; plastic deformation; microstructure

1 Introduction

In recent years, the automobile industry has gradually moved towards producing lighter vehicles with a higher fuel economy and a lower cost. Towards this goal, the development of high strength steel plates has been a major objective in the automobile and steel industries[1,2]. Hot rolled dual-phase (DP) steel is obtained by adjusting the cooling speed after rolling to control the phase composition and the volume fraction of each phase. Possible compositions include, ferrite + bainite (F + B), martensite and ferrite + pearlite and ferrite(F + M) + P (F), and ferrite + bainite + martensite (F + B + M), along with other possible compositions. This allows the strength and elongation rate to be tailored over a wide range and combined with the material's good initial strain hardening characteristics and high energy absorption ability. This not only meets the demands for altering the material's performance for different applications but can also simplify the production process and hence reduce its cost[3-5].

Research on the stress-strain relationship of DP steel is mainly concentrated on the constitutive relation with the high temperature and high strain rate model, and is used to study dynamic recovery and recrystallization. Sha Q[6] studied the process of low carbon steel static recrystallization and dynamic recrystallization. A $t_{0.5}$ equation was established that could reflect the microalloy elements generated in the solid solution by the solute drag effect. Yu F[7] calculated the sub-recrystallization temperature of high strength steel through single pass compression, continuous pass compression and stretch compression cycle experiments. In this manner they determined an optimized reduction and pass interval time to effectively control the refinement of the austenite grains. Dai QF[8] established the constitutive relationship of DP steel based on the Johnson-Cook constitutive model. This was accomplished by studying the effects of different strain rates on the deformation

(Received: Nov. 19, 2019; Accepted: Mar. 22, 2020)

PANG Qihang(庞启航):Ph D; Lecturer; E-mail: qihang25@163.com

*Corresponding authors: XU Zhen(徐振): Ph D; E-mail: ustlxuzhen@126.com; XU Mei(徐梅): Ph D; E-mail: xumei@tisco.com.cn

Funded by the National Natural Science Foundation of China (No. 52004122), the State Key Laboratory of Marine Equipment made of Metal Material and Application(No.SKLMEA-USTL-201906), the Guidance plan of Natural Science Foundation of Liaoning Province (No.2019-ZD-0025), and the Key Project of Liaoning Education Department (No.2019FWDF03)

of DP steel at ambient temperature; however, this model could not reflect the relationship between the microstructure and the macroscopic stress and strain directly. Pang QH[9] described the hot milk microscopic stress-strain model of dual phase steel; the uniaxial tensile curve of DP590 and DP780 steel was demonstrated and validated according to the intermediate mixed multiphase laws and swift equation. It was found that the microscopic stress-strain relationship model could illustrate the basic parameters of the hot rolled DP steel microstructure and macro mechanical properties of the inner link. In addition, it could provide an accurate description of material deformation behavior and predict the macro tensile curve. In the preceding research on DP steel, the microstructure, manufacturing process, strain hardening behavior and deformation mechanism have been generally studied under quasi-static tensile tests.

In addition, previous studies also revealed that in comparison to the quasi-static state, there are significant differences in the mechanical properties and deformation behavior under dynamic loading. Beynon[10] found that as the strain rate increased from 10^{-3} to 10^{2} s^{-1}, the strength of the DP500 and DP600 steels was enhanced and the strain hardening rate decreased. Slycken[11] studied the dynamic response of 0.18%C-1.56%Mn-1.73%Al-0.021%Si-0.018%P TRIP steel and found that it showed higher strength and elongation and better energy absorption compared to the quasi-static conditions. Researches[12-14] have shown that the reason for the formation of dynamic strain aging (DSA) is the interaction between the motion dislocation, solute atoms and the C-Mn atoms in the process of plastic deformation. Other researches[15-17] have proved that this phenomenon is also related to the strain rate, temperature and other conditions during plastic deformation.

Therefore, the aim of this study was to further understand the effects of the strain rate on the deformation micro-mechanism for DP steel with a typical duplex microstructure. In this paper, the DP steel Fe-0.15C-0.6Si-2.1Mn was the material of focus and the alteration of its mechanical properties under different strain rates was studied. The dynamic plastic deformation mechanism of DP1000 steel was explained with respect to its strain rate sensitivity index, activation volume, and dynamic factor.

2 Experimental

DP steel was smelted in a vacuum electromagnetic induction furnace under an argon atmosphere and cast into ingots. The chemical composition is shown in table 1. The ingot was forged with dimensions of 80 mm × 80 mm × 70 mm and then heated for rolling at 1 180 ℃ for 1.5 h. The rolling temperature was 1 100 ℃, after 7 hot rollings to 4 mm, the temperature dropped to 620 ℃-650 ℃ and the final rolling thickness was 1.6 mm. Then the heat treatment was carried out on a CAS-300III simulated continuous withdrawal experimental machine. The heat treatment process was as follows: the heating rate was increased to 750 ℃ at 10 ℃/s and maintained at the final temperature for 7 min, it was then cooled to room temperature at a rate of 10 ℃/s.

According to the national standards GB/T 228.1-2010 and GB/T 30069.1-2013, wire cutting was used to cut the plates samples for the tensile test. The tensile tests at different strain rates was carried out in a sans-cmt5105 microcomputer-controlled electronic universal testing machine and Zwick HTM16020 high-speed tensile testing machine. A JEM-2010 high resolution transmission electron microscope (HR-TEM) was used to observe and analyze the microstructure of the steel and its evolution after tensile deformation. The TEM samples were treated with a 5% perchloric acid anhydrous ethanol solution as an electrolyte. The TEM operating voltage was set at 200 kV.

3 Results

3.1 Mechanical properties

Fig.1 shows the engineering stress-strain curves and the mechanical properties of the DP1000 steel at different deformation rates in the elastic deformation stage, it can be seen that the stress increased rapidly with increasing amounts of deformation; however, the elastic modulus did not change significantly, indicating that it was not affected by the change in the strain rate. In the plastic deformation stage, the stress-strain curve of the test steel demonstrated sensitivity to a change in the strain rate; that is, with an increase in the strain rate, the yield strength and tensile strength increased. Fig.1(b) shows that the break elongation and uniform elongation of the DP1000 steel has a nonmonotonic

Table 1 The chemical composition of DP1000 steel/wt%

Elements	C	Mn	Al	Cr	Si	P	S	Fe
Tested steel	0.15	2.1	0.067	0.43	0.65	<0.01	<0.008	Balance

trend; when the strain rate increased from 10^{-3} s^{-1} to 10^{-2} s^{-1}, they were both almost the same. This is because in the early stages of plastic deformation, there is enough time for the internal material dislocation motion resistance to be released due to the low deformation rate. This results in elongation with no obvious changes to the deformation rate. When DP1000 steel has a low strain rate (10^{-2}-10^{0} s^{-1}) for deformation, there is an enhancement in inhomogeneous plastic deformation ability. The uneven plastic deformation ability decreases with increasing deformation rate, this is because that the resistance is too late to release by dislocation movement, causing a concentration of local stress. This produces inhomogeneous plastic deformation, causing a weakening of the uneven plastic deformation ability. At the same time, due to the strengthening effect of the high-density dislocations in ferrite, the difference in the plastic strain energy between the ferrite and martensite/ferrite interface is reduced, and the non-uniform plastic deformation capacity is enhanced to some extent. Subsequently, the elongation after fracture and the uniform elongation are both increased with increasing strain rate. They both began to decrease rapidly when the strain rate reached 10^{3} s^{-1}.

3.2 Microstructure

Fig.2 shows the original microstructure of DP1000 steel. As seen in Fig.2(a), the DP1000 steel shows a typical ferrite and martensite biphasic structure before deformation; the concave part is the F tissue and the convex part is the M tissue. Fig.2(b) displays the inverse pole figure (IPF) map, the average observed grain size was 5.13 ± 0.02 μm after the EBSD measurement.

Fig.3 shows the fine structure of the DP1000 steel at strain rates of 10^{-3}, 10^{0}, and 10^{3} s^{-1} before deformation. As can be seen from Fig. 3(a), the DP1000 steel contains short and coarse martensite laths, massive ferrite, and a small dislocation density before deformation. Plastic deformation occurred when the strain rate was 10^{-3} s^{-1}. The dislocation began to accumulate near the M/F interface and dislocation cells formed in the ferrite grains, as shown in Fig.3(b). On increasing the strain rate to 10^{0} s^{-1}, the dislocation cell size and dislocation density increased. The difference of plastic deformation energy between ferrite matrix and M/F interface is capable of decreased, and the formation and extension of micro cracks was delayed at the M/F interface[18]. This results in a simultaneous increase in the material's strength; in addition, the break

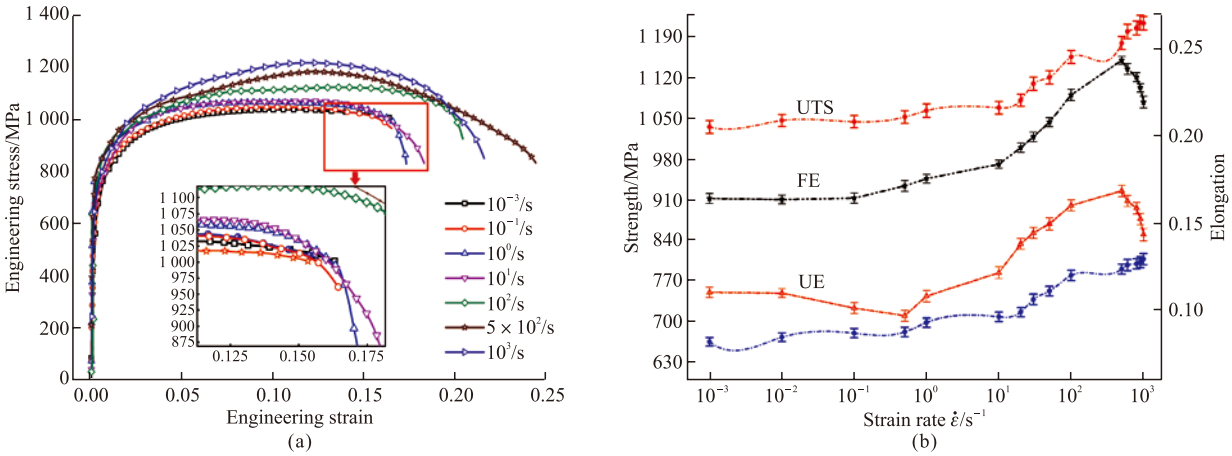

Fig. 1 Engineering stress-strain curves (a) and mechanical properties (b) of DP1000 steel at different strain rates

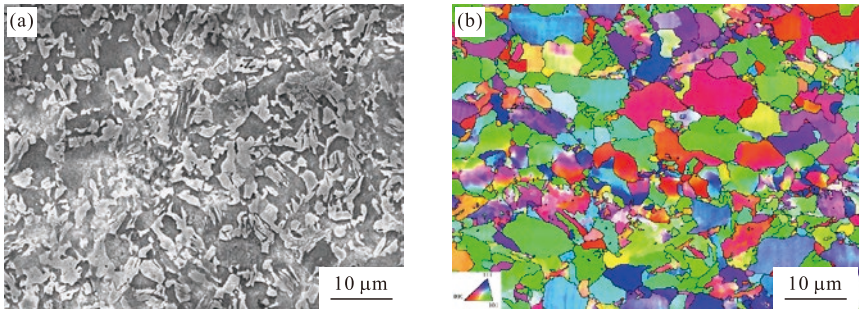

Fig. 2 Original SEM and EBSD morphologies of DP1000 steel: (a) SEM and (b) EBSD

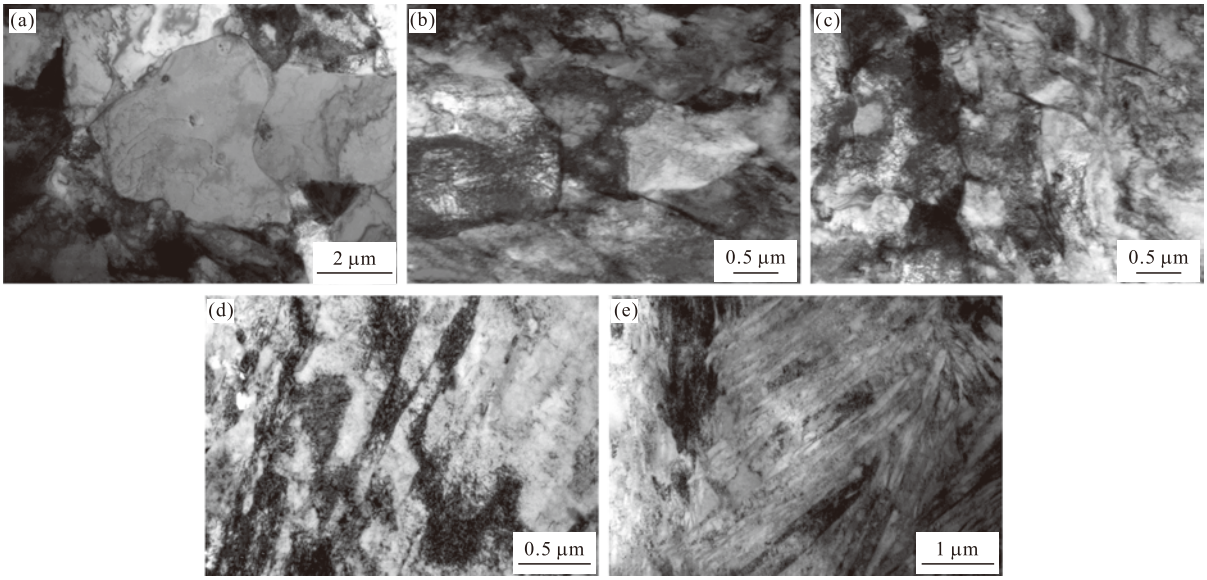

Fig.3 TEM images of DP1000 steel at different strain rates: (a) before deformation; (b) 10^{-3} s^{-1}; (c) 10^{0} s^{-1}; (d) 10^{2} s^{-1}; (e) 10^{3} s^{-1}

elongation increases slightly as shown in Fig.1(b) and Fig.3(c). When the strain rate increases, the ferrite formed an increased amount of dislocation tangles near the M/F interface. This results in the production of new dislocation cells due to the multiple slip systems occurring at the same time and an increase in the number of movable dislocation[19,20]. Therefore, the material's plasticity, its strength, and the work hardening ability become enhanced. On the other hand, it was observed in Fig.3(d) that the martensite lath elongated, this is due to the DP1000 steel being subject to a high rate of deformation. The M/F generated a lot of dislocations near the interface, resulting in premature martensite yield occurring and plastic deformation that coordinates the strain hardening of ferrite. For a large deformation and strain rate, a higher adiabatic temperature is generated, which leads to a temperature rise in M and make it more prone to plastic deformation. This also illustrates that in Fig.1(b), with the increase of the strain rate, the strain in the martensite begins to decrease by plastic deformation. With a further increase of the strain rate, the degree of dislocation entanglement and plugging becomes more intense. Hence, the softening effect caused by dislocations and the adiabatic temperature rise can no longer offset the hardening caused by the obstruction of the dislocation movement, resulting in the premature formation of microcracks within M[21] This results in M fragmentation, which reduces the plasticity of the material. In summary, the plastic deformation mechanism of DP1000 steel under dynamic loading is determined by the competitive results of the softening effects caused by work hardening (strain hardening and increasing the strain rate hardening) and the adiabatic temperature rise.

3.3 Strain hardening behavior

Fig.4 shows the work hardening curve of DP1000 steel under different strain rates. It can be seen from the figure analysis that the work hardening rate of DP1000 duplex steel shows three stages as the true strain increase. In stage I, compared with the quasi-static deformation condition (10^{-3}-10^{-1} s^{-1}), the work hardening rate decreased slowly as the true strain increased under high strain rate (10^{0}-10^{3} s^{-1}) deformation. This is because under a high rate of deformation, DP1000 martensite near the ferrite grain boundary in steel can produce a lot of dislocations, as the deformation degree increases the formation of new dislocations are hampered by grain boundaries. This can also be used as a source of new dislocations, causing an increased dislocation density around the martensite[22], which slows down the decline in the work hardening rate. In phase II, although the change in the work hardening rate with the increase of real variables should be slow; under dynamic loading conditions (10^{0}-10^{3} s^{-1}), the change in the work hardening rate with the true strain curve is obviously different from that of the low strain rate (10^{-3}-10^{-1} s^{-1}). Here a shorter curve of the platform is observed, and on increasing the strain rate, the platform appears earlier and is shorter. The platform then falls quickly into phase III until after sample fracture. The reason is that as the strain rate increases, the instantaneous plastic deformation of the material becomes larger, leading to an increase of the dislocation density. This makes slip dislocations more difficult, leading to a

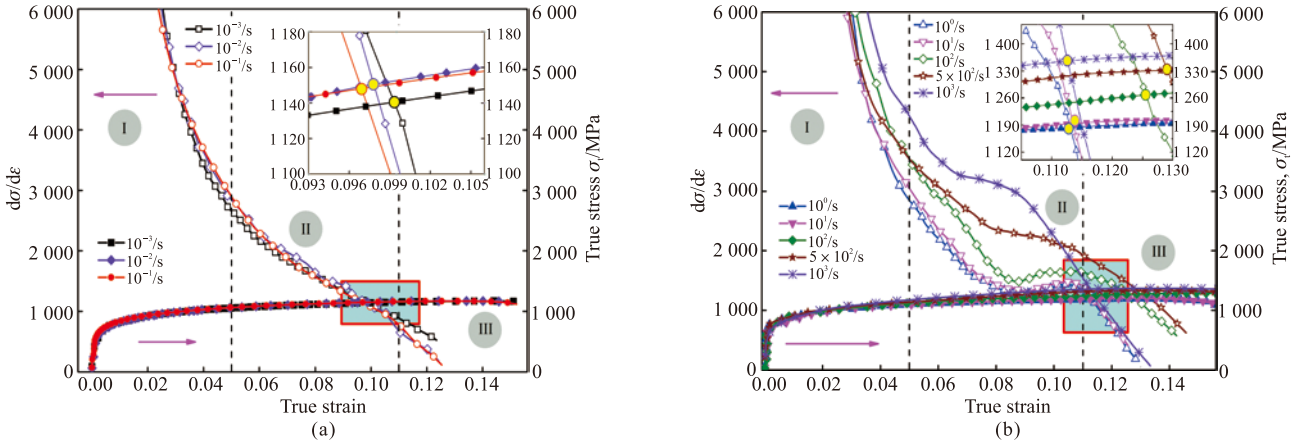

Fig.4 Work hardening curve of DP1000 steel at different strain rates

reduction of the hardening rate and the observed slowing or flat trend. However, the deformation of materials under high strain rates results in localization softening. This is coupled with the deformation process on adiabatic temperature rise, which causes the martensite temperature rise; thus, plastic deformation is more likely to occur. The yield of martensite and the common role of the dynamic response make DP1000 experimental steel under high strain rate enter more quickly into the rapidly reduced phase III.

According to Considère instability criterion[23], when a materials work hardening rate is equal to the true stress in the process of tensile deformation, plastic instability in the material will immediately occur. As seen in the enlarged inset on the upper right corner of Fig. 4, if the delay-work hardening rate curve intersects with the true stress-true strain curve (the intersection point is the instability point), the uniform elongation would increase. The obtained results are consistent with the analysis of the change in the uniform plastic deformation performance with the strain rate in the DP1000 steel. In other words, according to Considère instability criterion, the instability strain of the DP1000 duplex steel has a minor change under quasi-static (10^{-3}-10^{-2} s^{-1}) deformation conditions; it then slowly decreases under a low-medium strain rate (10^{-2}-10^{0} s^{-1}); increases under medium-high strain rate; and then decreases in the high strain rate range (5×10^{2}-10^{3} s^{-1}).

4 Discussion

4.1 Strain rate sensitivity index

Fig.5 shows the change of the true stress with the strain rate of DP1000 steel under different strain variables. Its slope is the corresponding SRS index m value for the two kinds of steel within a certain strain rate range, as shown in formula (1)[24, 25].

$$m=\frac{\partial \ln\sigma}{\partial \ln\dot{\varepsilon}} \tag{1}$$

where, σ is the rheological stress, and $\dot{\varepsilon}$ is the strain rate. The larger the m value, the stronger the anti-necking ability of the material, which results in delayed fracture.

From the slope of the curve in the Fig.5, it can

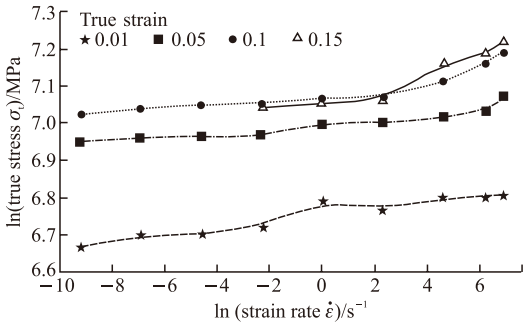

Fig.5 The log-log relationship between rheological stress and the deformation rate at different strain rates for DP1000

be seen that the value of the SRS index m for DP1000 steel are all positive but differ with different amounts of deformation. Under quasi-static (10^{-3}-10^{-2} s^{-1}) tensile conditions, for deformations of 0.01, 0.05, 0.1, 0.15, the value of m is almost unchanged. As the deformation increases to 0.15, with a low/medium strain rate (10^{-2}-10^{2} s^{-1}), the value of m with different deformations is larger. This indicates that high strength DP steel has a higher SRS. Under dynamic loading (10^{2}-10^{3} s^{-1}), the m value under small strain variables (0.05, 0.1) is comparable to that with a low and medium strain rate, and is much larger than the m value under strain rates of 10^{-3}-10^{-2} s^{-1}. The slope (m value) also increases with a large strain, indicating that DP1000 steel has a high strain rate sensitivity at high strain rates.

4.2 The activation volume

The strain rate sensitivity S[26] can be expressed as:

$$S = \frac{k_B T}{v^*} \tag{2}$$

where, k_B is the Boltzmann constant; T is the absolute temperature; $v^*$is the activation volume, It's defined as the derivative of activation enthalpy with respect to stress at a certain temperature[26], given by:

$$v^* = -\left[\frac{\partial \Delta H(\tau)}{\partial \sigma}\right]_T = k_B T\left(\frac{\partial \ln \dot{\varepsilon}}{\partial \sigma}\right) \tag{3}$$

where, $\Delta H(t)$ is the enthalpy of activation.

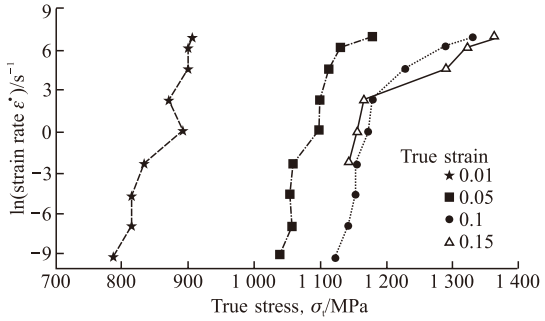

Fig.6 Relationship between the log of the strain rate and the rheological stress at different strain variables

Table 2 The value of the activated volume v^* in DP1000 steel at different stress variables (b^3)

$\dot{\varepsilon}$/s^{-1}	The true strain			
	0.01	0.05	0.1	0.15
10^{-3}-10^{3}	21.56			
10^{-3}-5×10^{2}		29.04		
10^{-3}-10^{1}			37.00	
10^{-1}-10^{1}				35.26
10^{1}-10^{2}			7.94	3.27
10^{2}-10^{3}			3.94	5.43
5×10^{2}-10^{3}		2.59		

Note: b is the order of magnitude of the berg vector

Fig.6 shows the relationship between the logarithm of the strain rate and the rheological stress of DP1000 steel under different strain variables. Table 2 shows the statistical table for the activated volume v^* of DP1000 steel under different strain rates. From Fig.6 and Table 2, it can be seen that when the deformation rate is relatively high (above 10^1 s^{-1}), the v^* value of DP1000 steel is relatively small, ranging from 2.59 to 7.94. Such a small activation volume indicates that DP1000 steel has a high strain rate sensitivity at higher strain rates when the deformation is relatively large, and is consistent with previous results. However, when it is less variable (such as true strain of 0.01), or the strain rate is low (such as 10^{-4}-10^1 s^{-1}) with a large deformation (such as true strain of 0.1), the activation volume v^* is relatively large. In other words, under a quasi-static or low strain rate, the strengthening of the strain rate effect is not obvious, Fig.1(b) shows the intensity with the variation of the strain rate.

4.3 Dynamic factor

Table 3 Statistics for the DP1000 steel strength dynamic factor under different engineering deformations

$\dot{\varepsilon}$/s^{-1}	Engineering strain				
	0.002	0.01	0.05	0.1	UTS
10^{-4}	1	1	1	1	1
10^{-3}	1.0107	1.0155	1.0143	1.0199	1.0147
10^{-2}	1.0228	1.0220	1.0205	1.0279	1.0255
10^{-1}	1.0335	1.0337	1.0348	1.0318	1.0236
10^{0}	1.0609	1.0415	1.0451	1.0498	1.0422
10^{1}	1.0761	1.0725	1.0707	1.0567	1.0472
10^{2}	1.1842	1.1529	1.1260	1.1025	1.1326
5×10^{2}	1.2009	1.1736	1.1639	1.1552	1.1562
10^{3}	1.2268	1.1995	1.2121	1.2121	1.1896

Note: the dynamic factors under each rate in this table are (engineering stress)/(engineering stress that corresponds to the strain rate of 10^{-4} s^{-1})

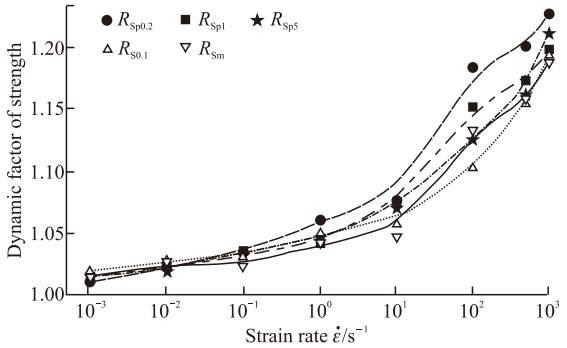

Fig.7 The dynamic factor for the strength of the DP1000 changes with strain rate at different deformations ($R_{Sp0.2}$: dynamic factor of the yield strength; R_{Sm}: dynamic factor of tensile strength; R_{Sp1}: the dynamic factor corresponding to the engineering stress when the engineering strain is 0.01; $R_{S0.1}$: the dynamic factor corresponding to the engineering stress when the engineering strain is 0.1)

Dynamic factor (R) is the ratio of dynamic intensity to quasi-static intensity[27]:

$$R = \frac{\sigma + \Delta\sigma}{\sigma} = 1 + \frac{\Delta\sigma}{\sigma} \tag{4}$$

where, the σ is under conditions of quasi static deformation intensity, $\Delta\sigma$ is the change in the intensity values. According to the above formula, the dynamic factor of the strength under different deformations (en-

gineering strain) is calculated. The trend of its change with the strain rate is shown in Fig.7. Table 3 shows the statistics of the dynamic strength factors for DP1000 steel under different engineering deformations. Where the dynamic strength factors involved are the ratio of engineering stress under a high strain rate, which corresponds to a deformation and engineering stress under 10^{-4} s^{-1}. From Fig.7 and Table 3, when the strain rate is less than 10^{-4} s^{-1}, the dynamic strength factor of DP1000 steel with different deformation amounts does not change significantly. Once the strain rate exceeds 10^{-4} s^{-1}, the dynamic factor for the yield strength is larger than those for the other deformation amounts. With the increase of the strain rate, the dynamic factor of the strength with different deformation quantities all increase rapidly. This indicates that at a higher strain rate, the enhancement of the rate is significant and the strain rate sensitivity is large. When the deformation rate ranges from 10^{-3}-10^{3} s^{-1}, the dynamic factors for the yield strength is greater than the dynamic factor for the tensile strength. This indicates that the strain rate sensitivity for the DP1000 steel yield strength is greater than that of tensile strength.

5 Conclusions

a) Under different strain rates, the tensile strength and yield strength of the DP1000 steel increases on increasing the strain rate. The elongation after fracture first increases without any change, and then rapidly declines when the strain rate increases to 10^{3} s^{-1}.

b) The work hardening rate and true strain curve of DP1000 steel show three stages. In the range of 10^{-3}-10^{-1} s^{-1}, the instability point is smaller; the instability point is larger in the range of 10^{0}-5×10^{2} s^{-1}, and the instability strain becomes smaller above 5×10^{2} s^{-1}.

c) The strain rate sensitivity index, activation volume and dynamic factor at three angles were used to analyze the DP1000 steel under different strain rates. The results show that the plastic deformation mechanism is made up of the competitive processes of work hardening and softening caused by the adiabatic temperature rise.

References

[1] Mozumder YH, Babu KA, Saha R, *et al*. Flow Characteristics and Hot Workability Studies of a Ni-containing Fe-Mn-Al-C Lightweight Duplex Steel[J]. *Mater. Charact.*, 2018, 146: 1-14

[2] Lei Y, Huang SY, Meng ZH, *et al*. Effects of Biaxial Tensile on the Deformation Behavior of DP590 High-strength Steel Sheet under High Strain Rate[J]. *J. Wuhan Univ. Technol. -Mater. Sci. Ed.,* 2017, 32 : 1 441-1 445

[3] Depover T, Vercruysse F, Elmahdy A, *et al*. Evaluation of The Hydrogen Embrittlement Susceptibility in DP Steel Under Static and Dynamic Tensile Conditions[J]. *Int. J. Eng. Sci.* 2019, 123: 118-125

[4] Nakada N, Tsukahara M, Fukazawa K, *et al*. Very Fine Structured DP steel with Tempered-martensite Matrix Fabricated by Fast Heating[J]. *Mater. Trans.* 2018, 59 : 166-171

[5] Zamani M, Mirzadeh H, Maleki M, *et al*. Enhancement of Mechanical Properties of Low Carbon Dual Phase Steel Via Natural Aging[J]. *Mater. Sci. Eng. A,* 2018, 734: 178-183

[6] Sha Q, Li D, Li G, *et al*. Dynamic and Static Recrystallization Behaviour of Coarse-Grained Austenite in a Nb-V-Ti Microalloyed Steel[J]. *J. Iron Steel Res. Int.* 2014, 21 : 233-239

[7] Fu Y, Yu H. Application of Mathematical Modeling in Two-Stage Rolling of Hot Rolled Wire Rods[J]. *J. Mater. Process. Tech.* 2014, 214 : 1 962-1 970

[8] Dai QF, Song RB, Guo Z. Research on Continuous Annealing Process of 1 000 MPa Cold-rolled Dual Phase Steel Using Orthogonal Design Method[J]. *Met. Sci. Heat Treat.* 2013, 55: 1-2

[9] Pang QH, Tang D, Zhao ZZ. Microstructure-based Model for the Stress--Strain Relationship of Hot-Rolled Dual-Phase Steel[J]. *J. Univ. Sci. Technol. B*, 2015, 37: 1 442-1 446

[10] Beynon ND, Jones TB, Fourlaris G. Effect of High Strain Rate Deformation On Microstructure of Strip Steels Tested Under Dynamic Tensile Conditions[J]. *Metal Sci. J*. 2013, 21:103-112

[11] Slycken JV, Bouquerel J, Verleysen P, *et al*. Static and Impact-dynamic Characterization and Modeling of Multiphase TRIP Steels[J]. *Mater. Sci. Forum*, 2009, 638: 3 585-3 590

[12] Beukel AVD. Theory of the Effect of Dynamic Strain Aging on Mechanical Properties[J]. *Phys. Status. Solidi. A*, 2010, 30: 197-206

[13] Beukel AVD, Kocks UF. The Strain Dependence of Static and Dynamic Strain-aging[J]. *Acta. Metall.* 1982, 30 : 1 027-1 034

[14] Wei W, Feng Y, Han L, *et al*. High-Temperature Low-Cycle Fatigue Behavior of HS80H Ferritic–Martensitic Steel Under Dynamic Strain Aging[J]. *J. Mater. Eng. Perform.* 2018, 27(7): 6 629-6 635

[15] Kang J, Wang C, Li YJ, *et al*. Effect of Direct Quenching and Partitioning Treatment on Mechanical Properties of a Hot Rolled Strip Steel[J]. *J. Wuhan Univ. Technol. (Mater. Sci. Ed.)*, 2016, 31: 178-185

[16] Li Z. Controlled rolling and cooling process for low carbon cold forging steel[J]. *J. Wuhan Univ. Technol. (Mater. Sci. Ed.)*, 2010, 25 : 89-93

[17] Tuğluca IB, Koyama M, Shimomura Y, *et al*. Lowering Strain Rate Simultaneously Enhances Carbon- and Hydrogen-Induced Mechanical Degradation in an Fe-33Mn-1.1C Steel[J]. *Metall. Mater. Trans. A*, 2019, 50 : 1 137-1 141

[18] Matsuno T, Teodosiu C, Maeda D, *et al*. Mesoscale Simulation of the Early Evolution of Ductile Fracture in Dual-phase Steels[J]. *Int. J. Plasticity.* 2015, 74 : 17-34

[19] Kapoor R, Nemat-Nasser S. Comparison Between High and Low Strain-rate Deformation of Tantalum[J]. *Metall. Mater. Trans. A*, 2000, 31 : 815-823

[20] Johnston WG, Gilman JJ. Dislocation Velocities, Dislocation Densities, and Plastic Flow in Lithium Fluoride Crystals[J]. *J. Appl. Phys.* 1959, 30 : 129-144

[21] Azuma M, Goutianos S, Hansen N, *et al.* Effect of Hardness of Martensite and Ferrite on Void Formation in Dual Phase Steel[J]. *Mater. Sci. Tech.* 2012, 28 : 1 092-1 100

[22] Han HQ, Huo G, Li UY, *et al*. Microstructure and Property of Cold Rolled and Heat Treated DP Steel Microalloyed With Titanium[J], *J. Iron Steel Res*. 2009, 21 : 28-42

[23] Liang W, Murakawa H, Deng D. Investigation of Welding Residual Stress Distribution in a Thick-Plate Joint with an Emphasis on the Features Near Weld End-start[J]. *Mater. Design,* 2015, 67: 303-312

[24] J Si, Z Jia, Wang J, *et al*. Comparative Analysis of Cold-mixed Epoxy and Epoxy SBS-modified Asphalts: Curing Rheology, Thermal, and Mechanical Properties[J]. *Constr. Build Mater.* 2018, 176: 165-171

[25] Peng J, Li KS, Pei JF, *et al*. Temperature-dependent SRS Behavior of 316L and its Constitutive Model[J]. *Acta Metall. Sin.* 2018, 31 : 234-244

[26] Tanga M, Kubinb L P, Canovac G R. Dislocation Mobility and the Mechanical Response of BCC Single Crystals: a Mesoscopic Approach[J]. *Acta Mater.* 1998, 46 : 3 221-3 235

[27] Levi-Hevroni D, Kochavi E, Kofman B, *et al*. Experimental and Numerical Investigation on the Dynamic Increase Factor of Tensile Strength in Concrete[J]. *Int. J. Impact Eng.* 2018, 114: 93-104